https://doi.org/10.5194/egusphere-2024-294
Preprint. Discussion started: 13 February 2024

Tide-Surge Interaction near Singapore and Malaysia using a Semi-empirical Model

Zhi Yang Koh[1], Benjamin S. Grandey[1], Dhrubajyoti Samanta[2], Adam D. Switzer[2,3], Benjamin P. Horton[2,3], Justin Dauwels[4], Lock Yue Chew[1]

[1]School of Physical and Mathematical Sciences, Nanyang Technological University, Singapore
[2]Earth Observatory of Singapore, Nanyang Technological University, Singapore
[3]Asian School of the Environment, Nanyang Technological University, Singapore
[4]Department of Microelectronics, Faculty of Electrical Engineering, Mathematics, and Computer Science, Delft University of Technology (TU Delft), The Netherlands

Correspondence to: Zhi Yang Koh (kohz0034@e.ntu.edu.sg)

Abstract. Tide-surge interaction (TSI) plays a substantial role in determining the characteristics of surges over shallow regions. A variety of approaches have been used to study TSI globally, and TSI have been found to occur in Singapore and the east coast of Peninsular Malaysia. However, the characteristics of TSI in Singapore and the east coast of Peninsular Malaysia have yet to be studied in detail. We study the TSI at seven tide gauges along the east coast of Peninsular Malaysia and Singapore. Here, we propose a modified statistical framework that accounts for irregularity in the tidal cycle. We find evidence of TSI at all seven locations, with characteristics varying smoothly along the coastline: the highest non-tidal residuals are found to occur most frequently before tidal high water at the southern region of this coastline and in Singapore, both before and after tidal high water in the middle of the coastline, and after tidal high water at the northern region. We also propose a semi-empirical model to investigate the effects of tidal phase alteration, which is one the mechanisms of TSI. Results of our semi-empirical model reveal that tidal phase alteration caused by wind-driven surges is substantial enough to generate significant change in the timing of the largest surges.

Short summary

Identifying tide-surge interaction (TSI) can be a complex task. We enhance existing statistical methods with a more robust test that accounts for complex tides, and investigate the influence of tidal phase

https://doi.org/10.5194/egusphere-2024-294
Preprint. Discussion started: 13 February 2024

alteration on TSI using a semi-empirical model. We apply these techniques to tide-gauge records from the east coast of Singapore and Malaysia. We found TSI at all studied locations, and that tidal phase alteration can change the timing of large surges with minimal impact on their height.

1 Introduction

Coastal regions are vulnerable to the combined effects of tides and surges, which can induce significant sea-level variations and pose substantial risks to coastal communities and ecosystems (Hsiang et al., 2017; Diaz, 2016; von Storch et al., 2015; Hinkel et al., 2014). The height of large storm surges can be amplified by high tides if they coincide, increasing the risk of coastal flooding and threatening lives and properties. The likelihood and impact of such destructive events are further aggravated by sea-level rise (Sreeraj et al., 2022; Calafat et al., 2022; Marcos and Woodworth, 2017; Feng et al., 2015; Woodworth and Blackman, 2004). To identify the appropriate response to such events, we must understand the fundamental processes and their mutual interactions.

A dependence between tides and surges has long been noticed at coastal locations (Keers, 1968), and recognised to be caused by interaction between tides and surges (Pugh and Vassie, 1978; Wolf, 1978). This interaction is non-linear and can lead to complex coastal dynamics characterized by amplification or attenuation of water levels, which are influenced by local bathymetry, coastline geometry, and atmospheric conditions (Idier et al., 2019). Strong tide-surge interaction has been observed in shallow waters and estuaries (Wolf, 1981). The main mechanism behind tide-surge interaction is mutual phase alteration (Rossiter, 1961). The generation of surges over a water body is influenced by the depth of the water body. As changes in depth occur partially due to tides, the height of surges can be influenced by tides. The propagation speed of tides is also dependent on depth, which can change due to surges (Proudman, 1957, 1955). Further studies that analysed shallow-water equations along the coast found that the non-linear tide-surge interaction is caused by the advection term, non-linear bottom friction term, and the non-linear shallow water effects of the shallow-water equations (Zhang et al., 2021; Idier et al., 2012).

Studies of tide-surge interaction have employed a range of modeling approaches, including statistical methods (Arns et al., 2020; Haigh et al., 2010; Dixon and Tawn, 1994), numerical models (Costa et al., 2023; Yang et al., 2023; Horsburgh and Wilson, 2007; Prandle and Wolf, 1978), and

https://doi.org/10.5194/egusphere-2024-294
Preprint. Discussion started: 13 February 2024

analytical models (Horsburgh and Wilson, 2007). Horsburgh and Wilson (2007) provided a simple mathematical explanation for the abundance of large non-tidal residuals at timings halfway up the rising tide and down the falling tide. Dixon and Tawn (1994) proposed a statistical framework where they split the tidal range into five equiprobable bands and used a chi-square test to determine whether residuals above a height threshold fall uniformly into each band. Horsburgh and Wilson (2007) proposed a modified version of the framework where the tide is instead split into 13 hourly bands between 6.5 hours before and after tidal high water (HW).

Application of such frameworks revealed that extreme residuals are most often found 3–5 hours before HW in the Bay of Bengal (Antony and Unnikrishnan, 2013) and the North Sea (Horsburgh and Wilson, 2007), and typically about 2 hours before HW in the English Channel (Haigh et al., 2010). In China and New Zealand, observed tide-surge interaction varies along the coastline: the frequency of extreme residuals peaks before HW at certain locations, after HW at others, and is independent of tides at the remaining locations (Costa et al., 2023; Feng et al., 2019). Numerical models have shown that the inclusion of tide-surge interaction often results in better water level predictions, especially over coastal and shelf waters, whereas the omission of the interaction may lead to under or overestimation of surges at certain locations (Fernández-Montblanc et al., 2019; Idier et al., 2012). For example, Antony et al. (2020) showed that numerically modelled peak water levels generated during Cyclone Aila at the head of the Bay of Bengal would have been overestimated if tide-surge interaction was not simulated.

Tide-surge interaction in the regional waters surrounding Singapore has previously been studied using hydrodynamic models. Using the Finite Volume Coastal Ocean Model (Chen et al., 2003), Chen et al. (2012) found that tide-surge interaction is negligible during large surges and mainly contributes by altering the time of tidal high and low water. Using a multi-scale modelling approach, Kurniawan et al. (2015) found tide-surge interaction to be important when simulating non-tidal barotropic flow. Kurniawan et al. (2015) recommend the inclusion of tide-surge interaction in operational forecast models to produce more accurate tides and surges. When applying a data-driven modelling approach, Kurniawan et al. (2014) also found that the tidal cycle influences non-tidal residuals.

Here, we focus on investigating tide-surge interaction at seven tide gauge locations near Singapore and the east coast of Peninsular Malaysia using modified statistical methods and a new semi-empirical

https://doi.org/10.5194/egusphere-2024-294
Preprint. Discussion started: 13 February 2024

model. The typical wave height is 0.5–1.5 m (Yaakob et al., 2016; Marzin et al., 2015). Our analysis found that that tides in this region can reach 2.7–3.6 m and the largest non-tidal residuals over the past 30 years exceed 0.8 m. Understanding how these components interact and combine provides insight into the contributors to coastal water levels. Hydrodynamical processes have a strong influence on the water levels at the seven tide gauges (Tay et al., 2016; Luu et al., 2016; Kurniawan et al., 2015; Karri et al., 2014; Tkalich et al., 2013a; Chen et al., 2012). The seven gauges are located within the Sunda Shelf, which has typical depth of 40–80 m. The shallowness of this shelf likely enhances the interaction between tide and surge, and its expanse allows for phase changes in the tides to compound as the tide propagates across the shelf. Our research objectives are (1) examining the tide gauge records to characterise the tide-surge interaction at each individual tide gauge location and the spatial pattern across locations, and (2) explaining the observed interaction characteristics through a simple semi-empirical model.

We apply a modified version of the statistical method by Horsburgh and Wilson (2007) to determine the presence of tide-surge interaction at each tide gauge location and to characterise these interactions. The existing method groups residuals above a height threshold into 13 hourly bands between 6.5 hours before and after HW and compares the resulting distribution to the uniform distribution using a chi-square test. However, as the duration and skewness of the tidal cycle can vary from cycle to cycle, the uniform distribution is not the most suitable null distribution. Our key modification to the existing methodology is to replace the uniform distribution with a "No-TSI distribution" as the null distribution. Due to variation in the duration of each tidal cycle, the No-TSI distribution is generally not uniform. A distinction between the No-TSI distribution and a uniform distribution should be made especially at locations with mixed tides, where the duration of tidal cycles can vary significantly. We compare the tide gauge data to the No-TSI distribution using an exact statistical test using bootstrapping instead of the chi-square test. In addition, we propose a simple approach to compare the tide-surge interaction across locations that have different tidal characteristics (diurnal, mixed, semidiurnal).

We aim to provide an explicit explanation of the observed tide-surge interaction through our semi-empirical model by combining historical tide and surge data with winds, coastal geometry, and bathymetry. The semi-empirical model accounts for the mechanism of tidal phase alteration: wind-induced surges perturb the depth of the water body which influences the propagation speed of the tide.

https://doi.org/10.5194/egusphere-2024-294
Preprint. Discussion started: 13 February 2024

This results in differences between observed tides and tides predicted from harmonic analysis, which are detected as non-tidal residuals. We aim to use our model to show that this mechanism can significantly influence the timing of extreme residuals to produce signals of tide-surge interaction.

2 Data and methods

2.1 Tide gauge data, tides and residuals

Hourly water level from tide gauges at seven locations (Fig. 1) along the east coast of Peninsular Malaysia and Singapore are obtained from the University of Hawaii Sea Level Center (Caldwell et al., 2001). Details of the tide gauges are tabulated in Table 1. Observations have been made over at least 29 years at each location with a data completion rate of 95–99 %. The length of these records is close to the 30-year threshold typically considered the minimum length required for analysis of extreme sea levels (Rasmussen et al., 2018). Nonetheless, within Southeast Asia, these stations have some of the longest records.

To compute the tidal level and non-tidal residuals, we use the equation

$$X(t) = Z(t) + T(t) + R(t). \tag{1}$$

$X(t)$ is the hourly water level recorded by a tide gauge at time t. $Z(t)$ is the 1-year (8766-hour after accounting for leap years) moving average of $X(t)$. A 1-year window was chosen because intra-annual behaviour of residuals is well understood to be periodic due to seasonal variations, and its influence on residuals are of interest in this study (Tkalich et al., 2013b). The 1-year moving average is calculated only if at least 85 % of the data in the 8766-hour window is available. This reduces our usable data to 87–99 % across the seven locations. $T(t)$ is the tidal level which we estimate using UTide, a tidal harmonic analysis package implemented in Matlab (Codiga, 2011). $X(t) - Z(t)$ is split into two equal halves based on the start and end dates in Table 1 and used as inputs to UTide, as UTide does not recommend using records longer than 18.6 years as input. UTide was used to identify the amplitudes and phases of 66 tidal constituents with periods of up to 32 days through harmonic analysis. Constituents with a signal-to-noise

https://doi.org/10.5194/egusphere-2024-294
Preprint. Discussion started: 13 February 2024

ratio of at least 2 are used to construct $T(t)$. $R(t)$, the residual, is then estimated as $R(t) = X(t) - Z(t) - T(t)$. We denote the residual obtained through this procedure as R_{gauge}.

A summary of the tidal characteristics at the seven locations is tabulated in Table 2. The tides at these locations lie within the microtidal (<2 m) and mesotidal (2–4 m) ranges with diurnal tidal ranges of close to 2 m except at Cendering and Geting where diurnal tidal ranges are 1.5 m and 0.8 m respectively. The daily tidal range can be as large as 3.6 m at Johor Baharu and Kuantan. In a shelf with a depth of 40–80m, tides of such magnitude cause water depth to deviate from its mean by up to about ±4 %. The periodicity of tides at a location can be described by the tidal form factor F which compares the relative importance of the following diurnal and semidiurnal tidal constituents (Pugh and Woodworth, 2014a):

$$F = \frac{K_1 + O_1}{M_2 + S_2}. \tag{2}$$

A common classification considers a location with a factor of <0.25 to be semidiurnal, 0.25–1.50 to be mixed with mainly semidiurnal tides, 1.50–3.00 to be mixed with mainly diurnal tides and >3.00 to be diurnal (Pugh and Woodworth, 2014a). Based on this classification, the tides at all stations are identified to be mixed, with Cendering and Geting being mainly diurnal while all other stations to the south are mainly semidiurnal.

2.2 Identifying tide-surge interaction

To determine whether tide-surge interaction is present at each of the seven tide gauge locations, we apply a modified version of the statistical method by Horsburgh and Wilson (2007) on the processed tide gauge records (Sect. 2.1). This method compares the timing of extreme residuals to the nearest HW.

To identify extreme residuals, the 99th percentile and above of residuals are longlisted. There are many clusters of residuals in the longlist, where the residuals within each cluster are consecutive measurements, each measured 1 hour from the last. The largest residual in each cluster is shortlisted and sorted. Starting from the largest, shortlisted residuals are added to the set of extreme residuals unless the residual was measured within 1 week (168 hours) of another extreme residual within the set. Some other thresholds used in published studies range from 12–60 hours (Arns et al., 2020; Feng et al., 2019;

Rasmussen et al., 2018; Buchanan et al., 2016; Horsburgh and Wilson, 2007). We choose a threshold of 168 hours to reduce the odds of double counting long-lasting surges while still retaining enough observations to infer statistical conclusions.

To compare locations with predominantly semidiurnal tides with locations with predominantly diurnal tides, we split the extreme residuals into two groups. We define a tidal cycle as the duration from one local minima in $T(t)$ to the observation immediately preceding the next local minima as illustrated in Fig. 2b. One group of extreme residuals were observed during tidal cycles of 21 hours or shorter, representing extreme residuals that occurred during semidiurnal cycles. The other group contain extreme residuals observed during tidal cycles of at least 22 hours, representing extreme residuals that had occurred during diurnal tides. This separation between 21-hours-or-less and 22-hours-or-more was chosen based on the characteristics of the duration of tidal cycles at the seven locations, where the distribution of the duration of tidal cycles were found to be bimodal at each location and the 22-hour mark tends to distinguish the two modes (Fig. S1).

The HW in the same tidal cycle as each extreme residual is identified and the timing difference between the extreme residual and the respective HW is quantified at hourly resolution. Across the set of extreme residuals, the frequency of extreme residuals found a certain number of hours relative to HW, h, is counted. This frequency is plotted as a *frequency distribution* in the form of a histogram (Fig. 3). Box plots below the histograms show the median and its 95 % confidence interval, the interquartile range (IQR), a range that extends up to 1.5×IQR from the limits of the IQR, and the outliers (Fig. 3).

We use the frequency distribution to test the null hypothesis that assumes that there is no tide-surge interaction. To do so, we test whether the frequency distribution is drawn from a null distribution representing a scenario where extreme events are equally likely to occur at any stage of a tidal cycle.

2.3 No-Tide-Surge Interaction distribution

In existing studies, a uniform distribution is chosen as the null distribution (Horsburgh and Wilson, 2007; Haigh et al., 2010; Antony and Unnikrishnan, 2013; Feng et al., 2019; Costa et al., 2023). However, the uniform distribution is not the most suitable null distribution to represent the null hypothesis. Instead, we propose a "No-Tide-Surge Interaction distribution" or "No-TSI distribution" as the null distribution. The

https://doi.org/10.5194/egusphere-2024-294
Preprint. Discussion started: 13 February 2024

No-TSI distribution is the *expected* frequency distribution in the absence of tide-surge interactions. Figure 2 illustrates how this distribution is obtained. The No-TSI distribution is empirically derived from $T(t)$, the tidal level obtained by applying UTide to the tide gauge records at each location. It is a distribution that depends on the local tidal characteristics and hence is location specific. For a given location, the null distribution is generally non-uniform because the length of the tidal cycle varies. For example, tidal cycles of 14 hours or longer are relatively rare at Tanjong Pagar, so randomly selected times that occur at 7 hours from the nearest tidal HW will also be relatively rare (Fig. 3a). This leads to non-uniform sampling of the number of hours from the nearest tidal HW. The No-TSI distribution corresponds to uniform sampling in time, which is non-uniform with respect to the number of hours from the nearest tidal HW. Thus, the No-TSI distribution is obtained by counting the number of tige-gauge observations found at a certain number of hours relative to HW as illustrated in Fig. 2.

The No-TSI distribution allows us to account for the complex mixed tides at each location, which causes the tidal cycles at the coast to have a period of any duration from 8 to 26 hours (Fig. S1). Let $f(h)$ be the number of tide gauge measurements collected at h hours from HW. Assuming independence between tide and surge, the probability that an extreme event will be found at h is $p_h = f(h)/\sum_h f(h)$: the normalized frequency of $f(h)$ at h. Note that p_h is a probability mass function over the domain h. Let n be the number of extreme events that occurred at this tide gauge over its length of records. Assuming that extreme events are mutually independent, the probability that k out of n extremes are found at h hours from HW is $C_k^n {p_h}^k (1-p_h)^{n-k}$ where C_k^n is the binomial coefficient. This is the binomial distribution $\sim \mathrm{Bin}(n, p_h)$. The No-TSI distribution at h is the mean of this binomial distribution, np_h. This means that the No-TSI distribution is the probability mass function p_h multiplied by n, and conversely p_h is the normalized No-TSI distribution such that $\sum_h p_h = 1$. We use the 2.5th and 97.5th percentiles of the binomial distribution at each h to obtain the 95% confidence interval of the No-TSI distribution. For testing the null hypothesis, a bootstrapping method is used to calculate p-values (Appendix A).

https://doi.org/10.5194/egusphere-2024-294
Preprint. Discussion started: 13 February 2024

2.4 Semi-empirical model

One effect of tide-surge interaction is tidal phase alteration, where surge-caused increase in water depth advances the timing of HW. The aim of our semi-empirical model is to investigate the first-order effects of phase alteration on the height and timing of residuals due to wind-driven surges. Singapore and the east coast of Peninsular Malaysia are located within the Sunda Shelf and lies to the west of the Riau Islands and southwest of the South China Sea (Fig. 1). The typical bathymetry of 40–80 m in this region of the Sunda shelf terminates at about 700 km away from the coast, declining steeply at the edge of the Sunda Shelf where it borders the South China Sea that have depths of 4,000 m and deeper. The unique topography of this region with an extensive area that is shallow and relatively uniform in depth has led us to adopt a simplified version of the sea-level gradient equation to estimate surge using wind velocity:

$$\frac{\partial \zeta}{\partial x} = \frac{\rho_{\mathrm{air}} C_d |\boldsymbol{W}| \boldsymbol{W} \cdot \hat{\boldsymbol{x}}}{\rho g D}, \qquad (3)$$

where we have assumed that the coastal sea is shallow enough to keep only terms with water depth in the denominator but is deep enough to justify ignoring bottom stress (Pugh and Woodworth, 2014b). In Eq. (3), ζ is the sea level and x is spatial displacement in a specified direction, making $\partial\zeta/\partial x$ the sea-level gradient along x. ρ_{air} is the density of air, C_d is the drag coefficient at the sea surface, ρ is the density of seawater, g is the gravitational acceleration, D is the undisturbed water depth, $\boldsymbol{W}$ is the wind velocity vector, and $\hat{\boldsymbol{x}}$ is a unit vector parallel to x. Winds over central South China Sea have been found to be the main determining factor of hourly water level variations in the Singapore Strait (Tkalich et al., 2013a). To compare the wind-driven surge at the seven tide gauge locations of interest, we assume that the surges at these locations result from winds over the same region of the shallow shelf. For our semi-empirical model, we use the region that is bounded by the red rectangle in Fig. 1, masking out land. A rectangular region was chosen for simplicity, with one edge passing through the Tanjong Pagar and Geting gauge locations and the remaining three edges encompassing as much of the shallow shelf as possible. The edges of the rectangle parallel to the Malaysian coast are roughly 833 km long and are separated by a longitude of 6.5°, making the edges perpendicular to the coast roughly 759 km long. Note that x in Eq. (3) is defined

https://doi.org/10.5194/egusphere-2024-294
Preprint. Discussion started: 13 February 2024

to be parallel to these perpendicular edges. Using bathymetry from the General Bathymetric Chart of the Oceans (GEBCO Compilation Group, 2023), we find that $D = 58$ m within the bounded region (after masking out grid boxes over land). This was obtained by averaging the bathymetry values within the red rectangle (Fig. 1). In this region, $g = 9.78$ ms^{-2}.

To estimate the wind-driven surge, we assume that ρ_{air}, C_d, ρ, g and D are spatially and temporally homogeneous over the bounded region and that C_d is independent of wind speed (Wróbel-Niedzwiecka et al., 2019). We also assume that the spatial average of $\boldsymbol{W}$ captures the first-order influence of regional winds on surge through averaging the wind components over the bounded region. These approximations allow us to easily integrate Eq. (3) with respect to x over the length of $L_{\mathrm{wind}} = 759$ km to estimate the wind-driven surge. Surges are not only a product of instantaneous winds but are also partially a result of winds over a past number of hours. To account for the time taken for the winds over the bounded region to cause surges at the tide gauge locations, we use a 25-hour running average of $|\boldsymbol{W}|\boldsymbol{W} \cdot \hat{\boldsymbol{x}}$ to estimate the wind-driven surge. The 25-hour averaging also serves to average out the dependence of D on tides, providing additional justification on our homogeneity assumption of D. Based on those assumptions, we estimate the wind-driven surge, R_{wind}, as:

$$R_{\mathrm{wind}} = \frac{\partial \zeta}{\partial x} L_{\mathrm{wind}} = k L_{\mathrm{wind}} \overline{|\langle \boldsymbol{W} \rangle_A| \langle \boldsymbol{W} \rangle_A \cdot \hat{\boldsymbol{x}}}, \tag{4}$$

where $\boldsymbol{W}$ is the wind velocity with its zonal (u) and meridional (v) components obtained from the hourly 10m winds of ERA5 (Hersbach et al., 2018), $\langle \boldsymbol{W} \rangle_A$ represents a spatial average of $\boldsymbol{W}$ over the area bounded by the red rectangle in Fig. 1 (after masking out grid boxes over land), $\hat{\boldsymbol{x}}$ is a normal vector along x pointing towards the Malaysian coast as shown in Fig. 1, $\overline{|\langle \boldsymbol{W} \rangle_A| \langle \boldsymbol{W} \rangle_A \cdot \hat{\boldsymbol{x}}}$ represents a 25-hour moving average of $|\langle \boldsymbol{W} \rangle_A| \langle \boldsymbol{W} \rangle_A \cdot \hat{\boldsymbol{x}}$, and $k = \rho_{\mathrm{air}} C_d / \rho g D$. Plotting $\overline{|\langle \boldsymbol{W} \rangle_A| \langle \boldsymbol{W} \rangle_A \cdot \hat{\boldsymbol{x}}}$ against R_{gauge}, the residuals obtained empirically from tide gauges (Sect. 2.1), at all seven locations reveal a correlation of 0.7–0.8 (Fig. S2). This leads us to fit the running average of $\overline{|\langle \boldsymbol{W} \rangle_A| \langle \boldsymbol{W} \rangle_A \cdot \hat{\boldsymbol{x}}}$ to the residuals using a simple linear regression to obtain the constant k and our estimate for R_{wind} at each location.

https://doi.org/10.5194/egusphere-2024-294
Preprint. Discussion started: 13 February 2024

With the speed of tidal waves given by $c = \sqrt{gD}$ (Pugh and Woodworth, 2014b) and treating R_{wind} as a perturbation to the undisturbed water depth D, the tide advancement time caused by a change in D due to R_{wind} is

$$\Delta t = \frac{L_{\mathrm{tide}}}{\sqrt{gD}} - \frac{L_{\mathrm{tide}}}{\sqrt{g(D+R_{\mathrm{wind}}/2)}} \approx \frac{L_{\mathrm{tide}}}{\sqrt{gD}}\frac{R_{\mathrm{wind}}}{4D}, \tag{5}$$

where L_{tide} is the distance travelled by the tidal wave under the influence of R_{wind}. The approximation assumes that $R_{\mathrm{wind}} \ll D$. We also assume that the tides travel straight towards the coast in the direction of $\hat{\boldsymbol{x}}$, allowing us to equate $L_{\mathrm{tide}} = L_{\mathrm{wind}}$. We then calculate the effects on residual height due to tide advancement from R_{wind} as $R_{\mathrm{phase}} = T(t + \Delta t) - T(t)$. R_{phase} can be viewed as a phase shift in the tidal levels, where extreme R_{phase} tend to cluster on the rising or falling tides instead of during tidal high or low water (Horsburgh and Wilson, 2007). Finally, we use the procedure described in Sect. 2.2 to obtain the timing of extreme R_{wind}, R_{phase} and $R_{\mathrm{sum}} = R_{\mathrm{wind}} + R_{\mathrm{phase}}$ relative to HW and their frequency distributions.

3 Results and discussion

3.1 Observed tide-surge interaction

We found evidence of tide-surge interaction at each location, where the frequency distributions deviate significantly from their respective No-TSI distribution (Fig. 3). Based on how we have defined extremes, we find that extreme residuals are unlikely to happen close to HW. This means that while the residuals exceeding the 99th percentile can occur close to HW, the peak of each cluster of exceedances is unlikely to be found in the time window close to HW. Across the locations, this time window generally begins 2–3 hours before HW and ends 3–5 hours after HW. Beyond this time window, the frequency of extreme residual increases, giving us frequency distributions that are mostly bimodal. At the four southernmost stations, the primary mode is found before HW: at -5 hours at Tanjong Pagar and Sedili, at -6 hours at Johor Baharu and at -7 hours at Tioman. Outside Southeast Asia, similar signals have been found at Port

https://doi.org/10.5194/egusphere-2024-294
Preprint. Discussion started: 13 February 2024

Otago in New Zealand (Costa et al., 2023), Shijiusuo, Lianyungang and Xiamen along the coast of China (Feng et al., 2019), Hiron Point at the Bay of Bengal India (Antony and Unnikrishnan, 2013), and Aberdeen, North Shields, Immingham, Cromer and Sheerness at the North Sea (Horsburgh and Wilson, 2007). At Kuantan, Cendering and Geting, the primary mode is found after HW, at +6, +6 and +4 hours respectively. Outside Southeast Asia, such signals have appeared less commonly but have been found at Onehunga in New Zealand (Costa et al., 2023) and at Kaohsiung and Zhapo in China (Feng et al., 2019).

In a separate quantitative test, we perform significance testing using the bootstrapping method described in Appendix A with 1,000,000 bootstrap samples. To account for family-wise error rate due to our multiple comparisons at seven locations, we apply the Bonferroni correction to our chosen significance level of 0.05 and require a p-value below $0.05/7 = 0.007$ to reject the null hypothesis. We find that the p-value of obtaining the frequency distribution from the No-TSI distribution is below the required level at all seven locations, allowing us to reject the null hypothesis that the frequency distribution was drawn from the No-TSI distribution at a significance level of 0.05 (Fig. S3). This provides further evidence supporting the presence of tide-surge interaction during semidiurnal tides at all seven tide gauge locations studied.

Comparing our results from the seven tide gauges along the Singapore and Malaysian east coast, we find a spatial pattern in the tide-surge interaction. At the southernmost stations of Tanjong Pagar, Johor Baharu and Sedili, the mass of the frequency distribution is heavily concentrated around their primary modes, which are found before HW. At Tioman, the primary mode is still found before HW, but the secondary mode has a distinctly heavier weight than the previous three stations. At Kuantan, tide-surge interaction has crossed over to another regime where the primary mode occurs after HW, but the secondary mode found before HW still carries comparative weight. At Cendering and Geting, the northernmost stations, the primary mode after HW is much heavier than the secondary mode before HW. This spatial pattern can also be seen using the box plots, which are compiled in Fig. 4. The tight interquartile range at Tanjong Pagar, Johor Baharu and Sedili shows that the mass of their frequency distributions is concentrated at -6 to -4 hours relative to HW. The larger interquartile range at Tioman shows that there is a more equal mass between the two modes, with the median at -5 hour revealing that the distribution is still heavier towards the negative values. The opposite is true at Kuantan, with its similar

https://doi.org/10.5194/egusphere-2024-294
Preprint. Discussion started: 13 February 2024

interquartile range to Tioman but with its median at +0.5 instead. At Cendering and Geting, the lower quartile is closer to HW, showing that the difference in relative mass between the two modes has increased.

During diurnal tides, we found no extreme residuals at Tanjong Pagar, Johor Baharu and Sedili. Few extreme residuals were found during diurnal tidal cycles at Tioman and Kuantan, while many were found at Cendering and Geting (Fig. S4). This is expected as Cendering and Geting experience mainly diurnal tides, in contrast to the other locations. Two observations are available at Tioman, which are too few to confidently determine the presence ofs tide-surge interaction even though both observations were found at least 6 hours after HW. The same can be said for Kuantan, where seven observations are available and were mostly found at least 6 hours after HW. Nonetheless, we calculate their p-values and compare them to $0.05/4 = 0.0125$. We find that their p-values are insufficient to reject the null hypothesis that the observed frequency distribution was drawn from the No-TSI distribution at a significance level of 0.05 and fails to provide evidence of tide-surge interaction during diurnal tidal cycles at these two locations. At Cendering and Geting, we continue to see the pattern where extreme residuals are unlikely to happen close to HW. This leads to a bimodal distribution with the primary modes at both locations found after HW, like their semidiurnal counterparts. The mode is 14 hours after HW at Cendering and 13 hours after HW at Geting. Respective p-values provide evidence of tide-surge interaction at both locations (Fig. S5).

3.2 Semi-empirical model results

We obtain R_{wind} by fitting $\overline{|\langle \boldsymbol{W} \rangle_A| \langle \boldsymbol{W} \rangle_A \cdot \hat{\boldsymbol{x}}}$ to the tide gauge residuals as described in Sect. 2.4. R_{wind} has a correlation of 0.7–0.8 with the tide gauge residuals (Fig. S2). This corresponds to an explained variance (coefficient of determination) of 0.5–0.6. This suggests R_{wind} is an adequate proxy of wind-induced surges.

We obtain the timing of extreme R_{wind} using the procedure described in Sect. 2.2 and compare it to its No-TSI distribution to determine whether there is any dependence between R_{wind} and tide. The reason for doing so is to show that the observed dependence between R_{gauge} and tide is not caused by any correlation between wind and tide, which are generated by independent processes. The validation of this

https://doi.org/10.5194/egusphere-2024-294
Preprint. Discussion started: 13 February 2024

assumption would imply that the observed dependence between R_{gauge} and tide is not caused by possible correlation to a common third independent variable, but that tide-surge interaction is indeed present. We find that the resulting frequency distributions for R_{wind} do not deviate significantly from their No-TSI distribution and provide no evidence of dependence between R_{wind} and tide (Fig. S6–S9), indicating the absence of such an independent variable.

To estimate the influence of tidal phase modulation, we compute Δt using Eq. (5) and then calculate $R_{\text{phase}} = T(t + \Delta t) - T(t)$ (Sect. 2.4). We apply the procedure of Sect. 2.2 to obtain the extremes of R_{phase} and find a clear dependence between R_{phase} and tide (Fig. S10–S13). During semi-diurnal tidal cycles, extreme values of R_{phase} are most found 2–4 hours before HW at all seven locations (Fig. S10). During diurnal cycles, extreme values are most found 3–5 hours before HW (Fig. S12). As with R_{gauge} and R_{wind}, no extremes were found during diurnal cycles at Tanjong Pagar, Johor Baharu and Sedili.

The prevalence of extreme R_{phase} within a narrow window of time relative to HW is due to R_{phase} being largest at 1/4 of a tidal cycle before HW, as illustrated in Fig. S14. As the natural period of a semi-diurnal tidal cycle is about 12–13 hours, a sinusoidal tidal waveform has the steepest gradients about 3 hours from its local maxima. This results in the tidal waveform having the greatest difference from a slightly horizontally displaced copy at close to 3 hours from HW. This mechanism is described in detail by Horsburgh and Wilson (2007).

However, extreme values of R_{phase} are not generally found at 6 hours before HW during diurnal tides. This is because a sinusoidal wave with amplitude A and frequency ω has a gradient that is proportional to the product $A\omega$. Since semidiurnal components of tides have about twice the frequency of their diurnal counterparts, diurnal constituents need to have at least twice the amplitude of semidiurnal constituents to have the same or stronger influence on R_{phase}. While the tides at Cendering and Geting are mainly diurnal, the amplitude of the diurnal constituents is less than twice that of the semidiurnal constituents (Table 2). Therefore, the semidiurnal signal has a stronger influence on the timing of extreme R_{phase}.

https://doi.org/10.5194/egusphere-2024-294
Preprint. Discussion started: 13 February 2024

We calculate $R_{\mathrm{sum}} = R_{\mathrm{wind}} + R_{\mathrm{phase}}$ and use the procedure outlined in Sect. 2.2 to find the timing of the R_{sum} extremes. The results during semidiurnal tidal cycles are shown in Fig. 5. The frequency distributions and p-values for R_{sum} suggest the presence of tide-surge interaction at Tanjong Pagar, Johor Baharu, Sedili, Tioman and Kuantan (Fig. 5 and S15). No significant interaction is identified at Cendering and Geting. This can also be seen in Fig. 4 where the medians of the frequency distributions at Cendering and Geting do not significantly differ from zero while the medians at the other five locations do. We find that the frequency distribution of R_{sum} has a single mode as opposed to the bimodal frequency distribution of the tide gauge residuals. At the five locations where R_{sum} provides an indication of tide-surge interaction, the modes of their frequency distributions of R_{sum} lie within 2–4 hours before HW, following R_{phase}. During diurnal tidal cycles, we find no evidence of tide-surge interaction (Fig. S16–S17).

We find that R_{phase} can significantly influence the distribution of the extreme values of R_{sum}. This is despite R_{phase} contributing to <1% of the variance of R_{sum} at all seven tide gauge locations (Fig. S18). By an alternative metric, the ratio between the standard deviation of R_{phase} and the standard deviation of R_{wind} is only 0–1%. Thus, while the magnitude of R_{sum} is effectively fully dependent on R_{wind}, the timing of its largest values is dependent on R_{phase}. We have shown that the process of tidal phase alteration—where wind-induced surges perturb the depth of the water body and influences the propagation speed of the tide—produces a significant and measurable tide-surge interaction at five locations. This result is complementary to Chen et al. (2012), who found that the influence of tide-surge interactions on large surges is negligible, although tide-surge interaction may alter the time of tidal high and low water.

However, our semi-empirical model is unable to accurately predict all the characteristics of tide-surge interaction found in R_{gauge} (Fig. 3). At Tanjong Pagar, Johor Baharu, Sedili and Tioman, extreme residuals typically occur even earlier than what our model suggests. Tidal phase alteration shifts the timings of extreme residuals towards times where tides are rising or falling the quickest, and no further. Our model is also unable to produce the bimodal distribution found in the tide gauge data illustrated in Fig. 3 and failed to produce statistically significant tide-surge interaction at Cendering and Geting. This

https://doi.org/10.5194/egusphere-2024-294
Preprint. Discussion started: 13 February 2024

suggests that the mechanism of tidal phase alteration cannot fully explain the observed tide-surge interaction and that additional explanations are required to fully account for the observations. One possible contributor is that shallower water during low tides can result in higher surges from near-shore winds (Pugh and Woodworth, 2014b). Kurniawan et al. (2014) had found that the tidal cycle influences non-tidal residuals. This could result in a further shift of the extremes towards tidal low water, which would be closer to the observed tide-surge interaction.

4 Conclusions

We have introduced the No-TSI distribution to be used in determining the presence of tide-surge interaction. The No-TSI distribution can account for irregular tidal cycles that can lead to non-uniform sampling with respect to the number of hours from HW. Hence, the No-TSI distribution is generally not a uniform distribution. When determining the presence of tide-surge interaction, the observed frequency distribution should be compared to the No-TSI distribution instead of a uniform distribution.

Analysis of tide gauge records using the No-TSI distribution provides evidence of tide-surge interaction at all seven tide-gauge locations along the Peninsular Malaysian east coast and Singapore. The observed interactions have a smooth spatial dependence along the coastline. During semi-diurnal tidal cycles at the southernmost location of Tanjong Pagar, extreme residuals are mostly found around 5 hours before tidal HW with a much smaller number of extremes occurring after HW. Moving northwards, similar patterns are found at Johor Baharu and Sedili, until we reach Tioman where extremes are mostly found before HW but many extremes can also be found after HW. Northwards from Kuantan, most extremes are found after HW.

To investigate the contribution of tidal phase alteration, we proposed a semi-empirical model. We used 10 m winds from ERA5 to estimate the effects of tidal phase alteration. At the five southern stations of Tanjong Pagar, Johor Baharu, Sedili, Tioman and Kuantan, we found the residual component caused by advancement of tidal HW can significantly alter the timing of extremes despite being responsible for less than 1% of the variance of the total residual. This demonstrates the effects of tidal phase alteration on the timing of extremes.

https://doi.org/10.5194/egusphere-2024-294
Preprint. Discussion started: 13 February 2024

Our model has explored one of the underlying mechanisms behind tide-surge interaction but is not designed to forecast water level or extreme events. A forecast model would require much more accurate modelling of the wind-driven surge. Inclusion of other underlying mechanisms of tide-surge interaction, such as the effect of tidal level on surge generation, would also be beneficial. Accounting for tide-surge interaction has been found to improve water level predictions in this region and other parts of the world (Antony et al., 2020; Fernández-Montblanc et al., 2019; Kurniawan et al., 2015; Idier et al., 2012). Knowledge of the interplay between tide-surge interaction and extreme sea levels can aid in the design of effective strategies for coastal planning, risk assessment, and mitigation measures, and will benefit from more comprehensive analyses. When studying extreme sea level in Southeast Asia, the relatively short length of available tide gauge records poses a challenge, providing a focus for further research.

Appendix A: Calculating p-value with bootstrapping

We label the *frequency distribution* obtained in Sect. 2.2 as $\boldsymbol{k}^{(\mathbf{0})}$. $\boldsymbol{k}^{(\mathbf{0})}$ is a function of h, the number of hours relative to HW. Consider the scenario where out of the n extreme events in $\boldsymbol{k}$, $k_0, k_1, k_2, \ldots$ number of events had occurred $0,1,2, \ldots$ hours after HW respectively and $k_{-1}k_{-2}, \ldots$ number of events had occurred $1,2, \ldots$ hours before HW respectively. The probability that this outcome is obtained from the No-TSI distribution is $p_{\{\boldsymbol{k}\}} = \frac{n!}{\prod_h k_h!}\prod_h p_h^{k_h}$ or $n!\prod_h p_h^{k_h}/k_h!$. This is a multinomial distribution. We label the *frequency distribution* of R_{gauge} as $\boldsymbol{k}^{(\mathbf{0})}$. For the bootstrapping procedure, we calculate $\log p_{\{\boldsymbol{k}^{(\mathbf{0})}\}}$: the log-probability of obtaining the *frequency distribution* of R_{gauge}, $\boldsymbol{k}^{(\mathbf{0})}$, from the normalised No-TSI distribution. To obtain a bootstrap sample, we then randomly draw n events from the normalised No-TSI distribution. We label the frequency distribution of this bootstrap sample as $\boldsymbol{j}^{(\mathbf{1})}$ and we calculate $\log p_{\{\boldsymbol{j}^{(\mathbf{1})}\}}$. Random draws are repeated 10^6 times until we obtain $\log p_{\{\boldsymbol{j}^{(\boldsymbol{m})}\}}$ for $1 \leq m \leq 10^6$. By the definition of p-values, we expect $p \times 10^6$ number of bootstrap samples to have a log-probability that is less than $\log p_{\{\boldsymbol{k}^{(\mathbf{0})}\}}$ and $1 - p \times 10^6$ number of bootstrap samples to have a log-probability of at least

https://doi.org/10.5194/egusphere-2024-294
Preprint. Discussion started: 13 February 2024

$\log p_{\{\boldsymbol{k}^{(0)}\}}$. Hence, the proportion of $\log p_{\{\boldsymbol{j}^{(m)}\}}$ that is less than $\log p_{\{\boldsymbol{k}^{(0)}\}}$ is the p-value representing the likelihood of the null hypothesis claiming absence of tide-surge interactions.

Code and data availability. The hourly tide gauge data can be downloaded from the University of Hawaii Sea Level Center (UHSLC) at https://uhslc.soest.hawaii.edu/data/?rq (Caldwell et al., 2001). The UTide MATLAB functions can be downloaded from https://www.mathworks.com/matlabcentral/fileexchange/46523-utide-unified-tidal-analysis-and-prediction-functions (Codiga, 2011). The ERA5 hourly data can be downloaded from https://doi.org/10.24381/cds.adbb2d47 (Hersbach et al., 2018). The bathymetry data can be downloaded from GEBCO at https://download.gebco.net/ (GEBCO Compilation Group, 2023). The analysis code used to produce the figures and tables can be downloaded from https://doi.org/10.5281/zenodo.10570585.

Author contributions. ZYK: conceptualisation; data curation; formal analysis; investigation; methodology; software; visualisation; writing – original draft preparation; writing – review and editing. BSG: conceptualisation; investigation; methodology; writing – review and editing. DS: writing – review and editing. ADS: conceptualisation; writing – review and editing. BPH: funding acquisition; supervision (supporting); writing – review and editing. JD: funding acquisition; supervision (supporting); writing – review and editing. LYC: funding acquisition; project administration; resources; supervision (lead); conceptualisation; investigation; methodology; writing – review and editing.

Competing interests. The authors declare that they have no conflict of interest.

Acknowledgements. This Research is supported by the National Research Foundation, Singapore, and National Environment Agency, Singapore under the National Sea-Level Programme Funding Initiative (Award No. USS-IF-2020-3). Any opinions, findings, conclusions, or recommendations expressed in this material are those of the author(s) and do not reflect the views of the National Research Foundation, Singapore, and the National Environment Agency, Singapore. This work comprises EOS contribution number XX (to be numbered).

https://doi.org/10.5194/egusphere-2024-294
Preprint. Discussion started: 13 February 2024

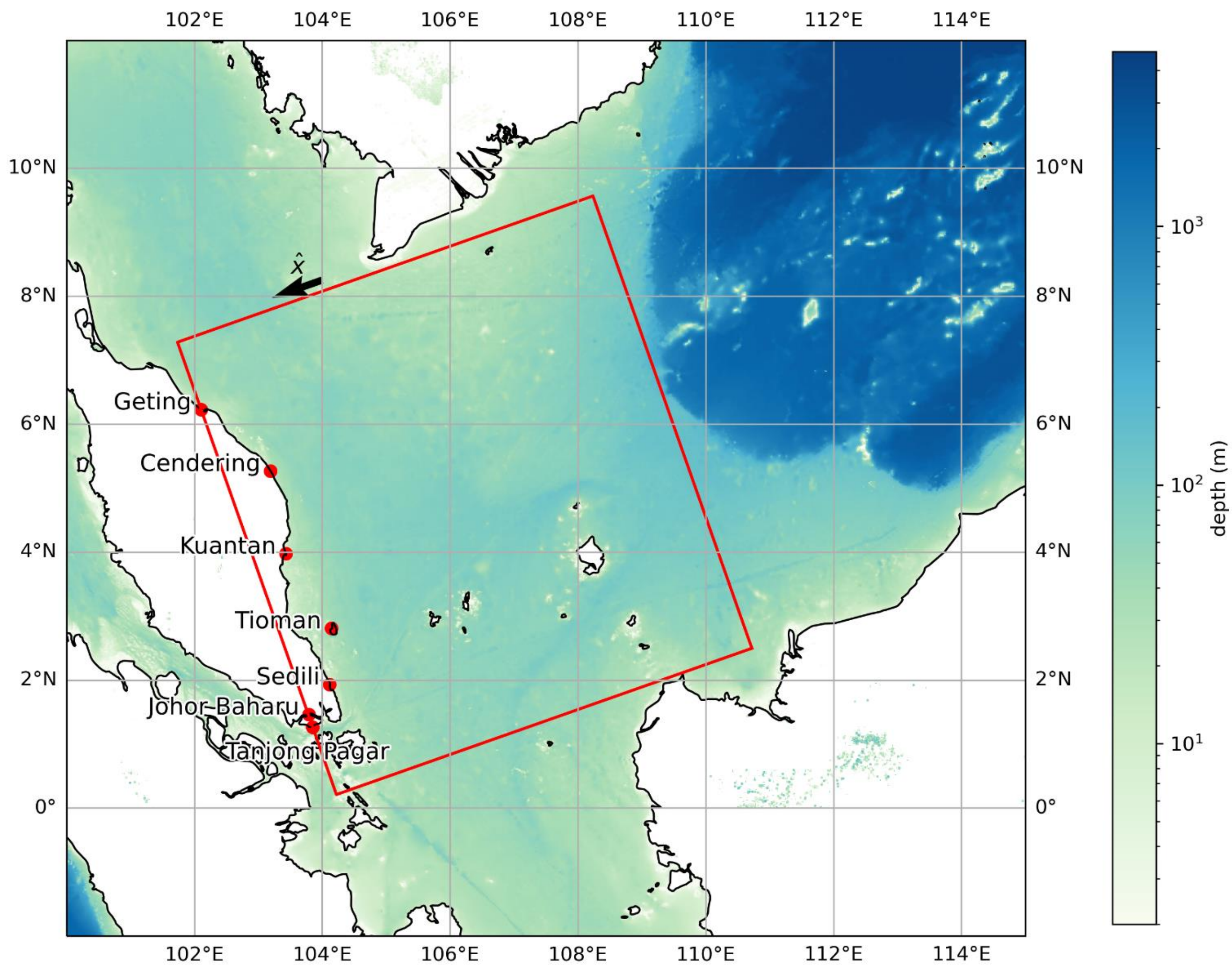

Figure 1: Bathymetry (in m) of the region of interest of this study, obtained from GEBCO, the General Bathymetric Chart of the Oceans (GEBCO Compilation Group, 2023). The seven tide gauge stations analysed are marked in red circles. The red rectangle denotes the region where 10 m winds are considered when calculating R_{wind} (Sect. 2.3). The region is roughly a rectangle of 759 km by 833 km. The unit vector $\hat{x}$ used in Eq. (3) is shown in the figure.

https://doi.org/10.5194/egusphere-2024-294
Preprint. Discussion started: 13 February 2024

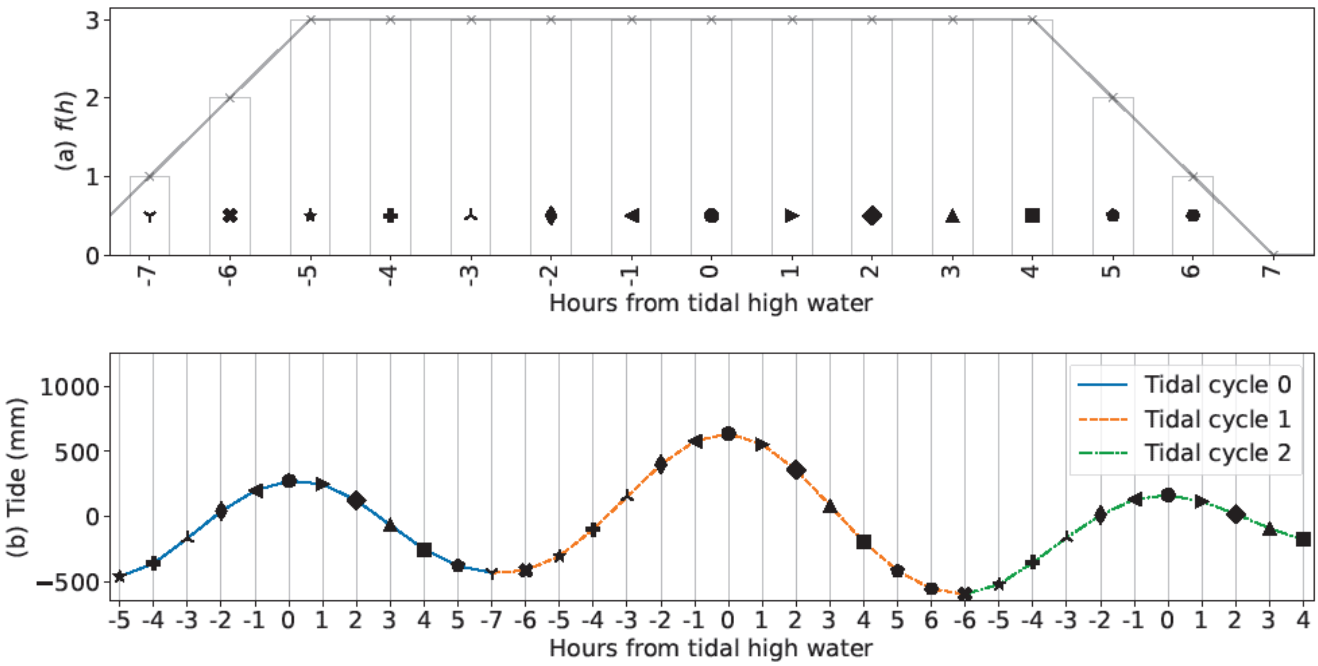

Figure 2: An example of how the No-TSI distribution is obtained, using three tidal cycles at Tanjong Pagar tide gauge station between 1 and 2 Jan 1989 (GMT). The number of hourly measurements made at h hours from HW are counted and denoted as $f(h)$, the No-TSI distribution before normalization and scaling by the number of events (Sect. 2.2). In this example, if an extreme residual can occur at any hour with equal probability, it will be 3 times more likely to happen at HW than at 7 hours before HW. This is observed from (b) where $-5 \leq h \leq 4$ occur thrice, $h = -6$ and $h = 5$ occur twice, and $h = -7$ and $h = 6$ occur once, resulting from the three irregular tidal cycles.

https://doi.org/10.5194/egusphere-2024-294
Preprint. Discussion started: 13 February 2024

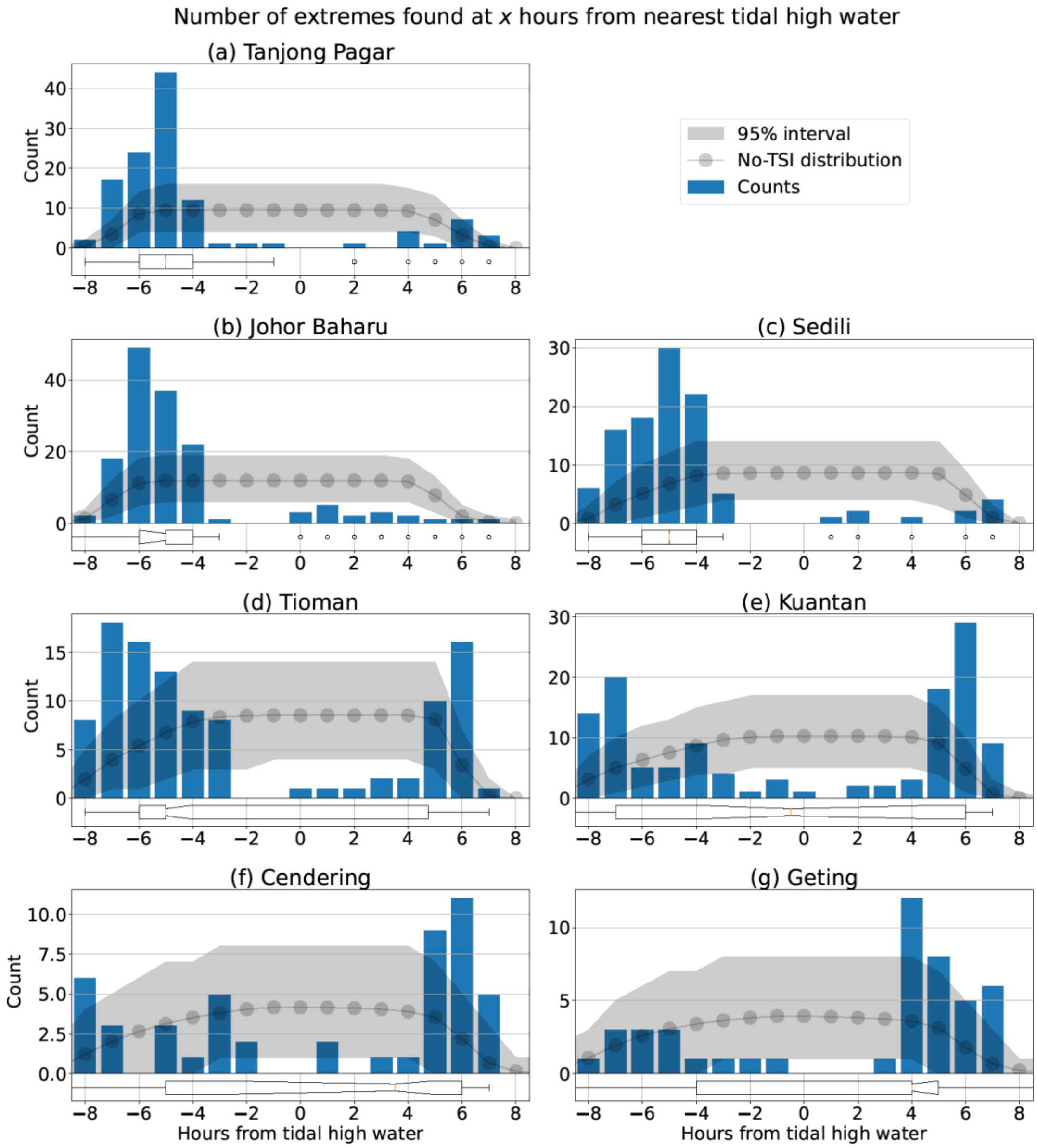

495

496 **Figure 3: Frequency distribution—the number of extreme events that have occurred at a certain**
497 **number of hours relative to HW—of extreme residuals (R_{gauge}) during semidiurnal tidal cycles**
498 **(Sect. 2.2). The plots are truncated at ±8 hours from HW. The frequency distribution is compared**
499 **to the No-TSI distribution, shown in grey, to determine the presence of tide-surge interaction (Sect.**
500 **2.2). Summary statistics of the frequency distribution are shown using the horizontal notched box**
501 **plot (Sect. 2.2). The whiskers of the box plot at (b) Johor Baharu, (e) Kuantan, (f) Cendering and**
502 **(g) Geting extend beyond ±8 hours from HW, and their full extent is shown in Figure 4.**

503

https://doi.org/10.5194/egusphere-2024-294
Preprint. Discussion started: 13 February 2024

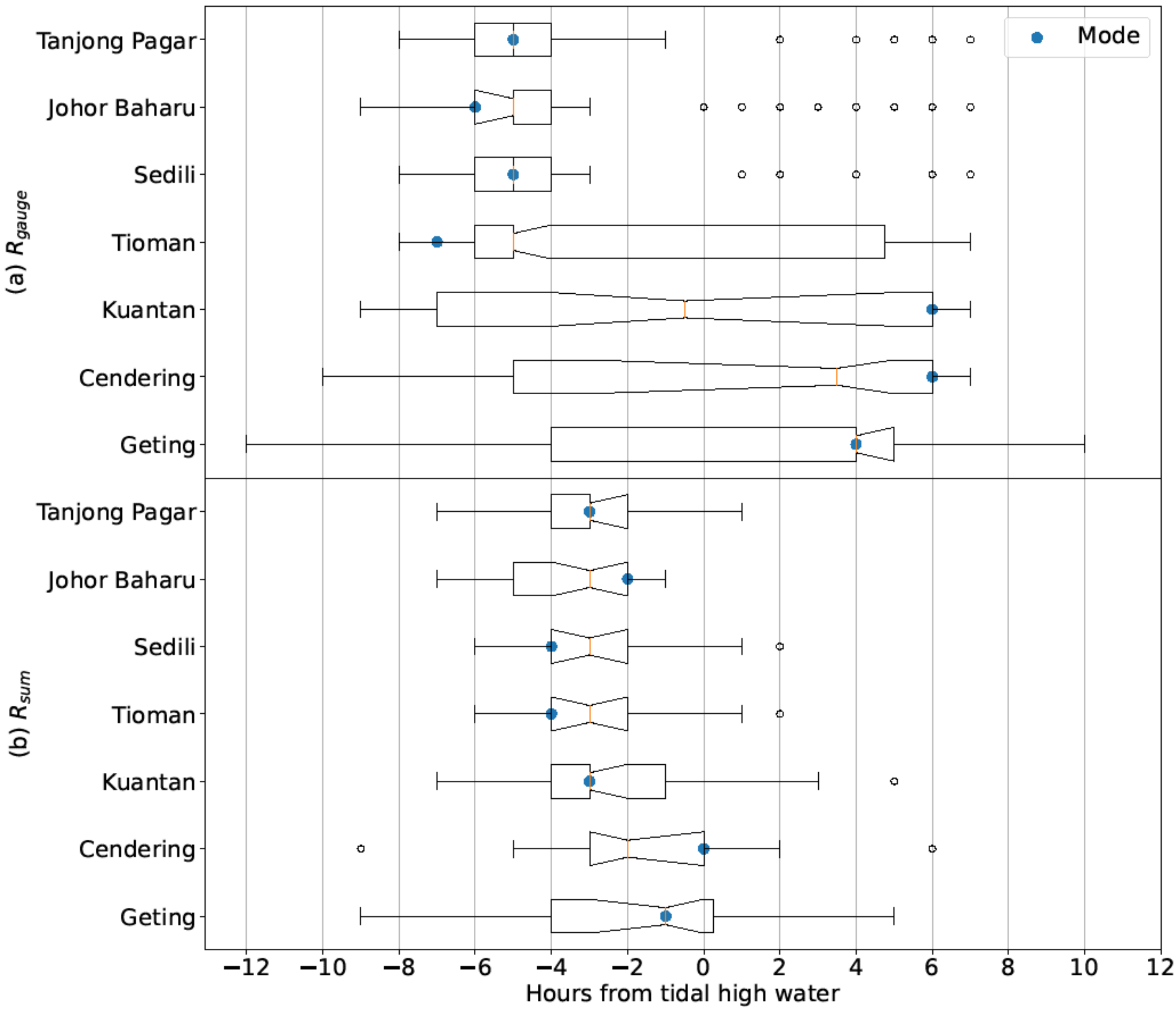

Figure 4: Compilation of the box plots in Fig. 3 and Fig. 5. Results presented in Fig. 3 on the timing of extreme residuals are compiled in subplot (a) and results presented in Fig. 5 on extreme values of R_{sum} are compiled in subplot (b). The box plots illustrate summary statistics of the distribution $k^{(0)}$ at each location, where orange lines indicate the medians, notches indicate the 95% confidence interval of the medians, blue circles indicate the modes, notched rectangles indicate the interquartile range (IQR), whiskers indicate a range that extends up to 1.5×IQR from the limits of the IQR, and black circles indicate outliers outside this range.

https://doi.org/10.5194/egusphere-2024-294
Preprint. Discussion started: 13 February 2024

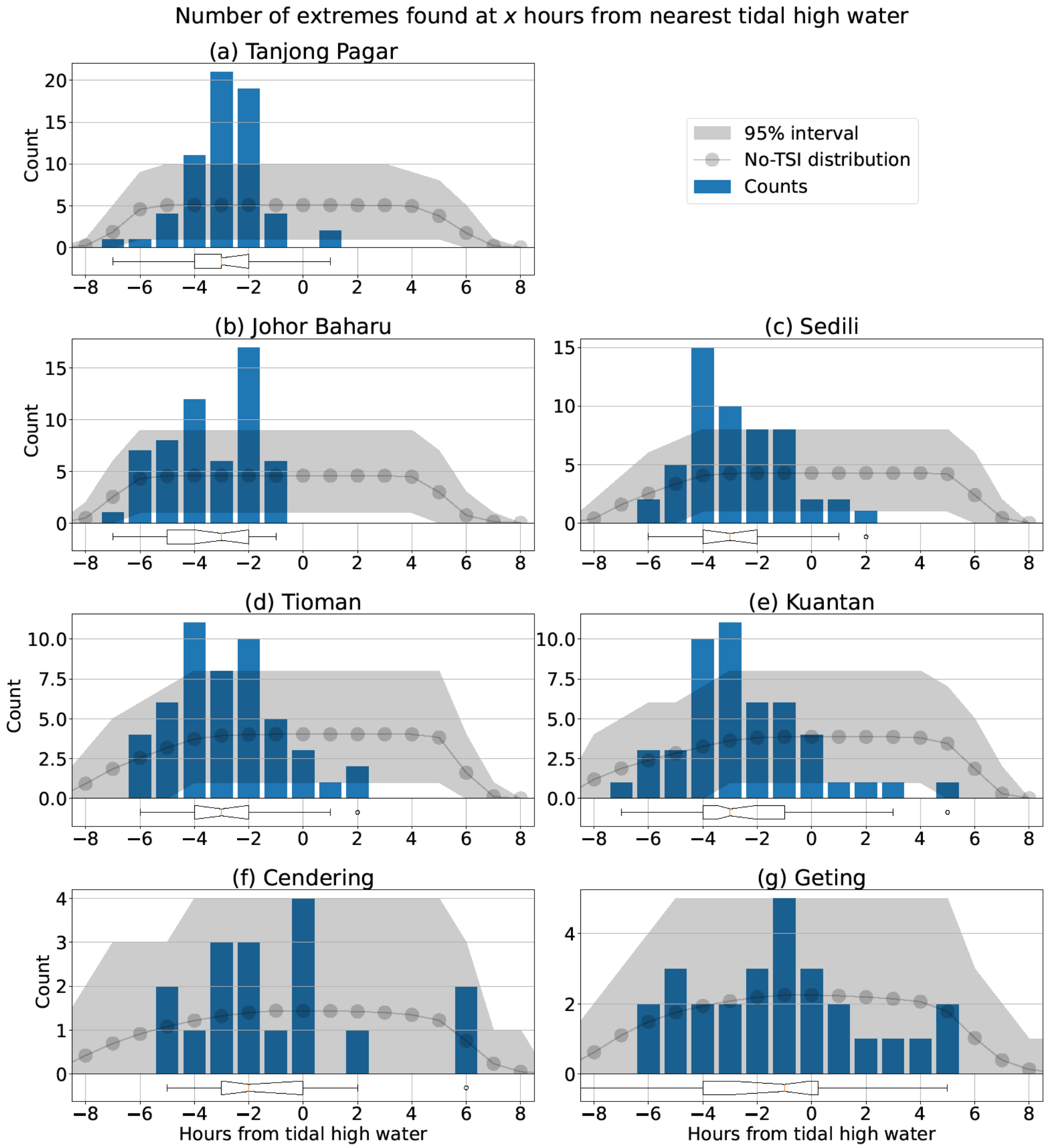

Figure 5: The frequency distribution for extreme values of R_{sum} and the No-TSI distribution during semidiurnal tidal cycles, truncated at ±8 hours from tidal HW. Truncated horizontal notched box plots illustrate some summary statistics of the frequency distribution, and their full extents are shown in Fig. 4.

https://doi.org/10.5194/egusphere-2024-294
Preprint. Discussion started: 13 February 2024

Table 1: Data availability of the tide gauges used in this study. Completion rate is the percentage of usable hourly observations out of the duration of records. Usable rate is the percentage of usable observations subtracting 1-year moving averages (Sect. 2.1).

Location	Latitude	Longitude	Start	End	Years	Completion (%)	Usable (%)
Tanjong Pagar	1.262	103.853	1988-01-01	2018-12-30	31.0	95.42	89.24
Johor Baharu	1.462	103.792	1983-12-19	2013-12-31	30.0	95.02	87.11
Sedili	1.932	104.115	1986-12-23	2015-12-09	29.0	98.08	98.08
Tioman	2.807	104.140	1985-11-13	2015-12-31	30.1	96.47	89.22
Kuantan	3.975	103.430	1983-12-22	2015-12-31	32.0	98.70	98.70
Cendering	5.265	103.187	1984-11-01	2015-11-30	31.1	96.58	90.58
Geting	6.227	102.107	1986-12-17	2015-12-31	29.0	99.14	99.14

https://doi.org/10.5194/egusphere-2024-294
Preprint. Discussion started: 13 February 2024

Table 2: Summary of the tidal characteristics at the study locations including tidal range, four tidal constituents (K_1, O_1, M_2, S_2), and the tidal form factor (F). Units, where applicable, are in metres (m). The diurnal tidal range is the difference between mean higher high water and mean lower low water, and is also referred to as the great diurnal tidal range or great diurnal range (NOAA, 2000). Maximum tidal range is the greatest difference between higher high and lower low water within a single day, and is much larger than the diurnal tidal range.

	Tidal Range						
Location	Diurnal	Max	K_1	O_1	M_2	S_2	F
Tanjong Pagar	2.2	3.3	0.31	0.30	0.80	0.32	0.54
Johor Baharu	2.4	3.6	0.31	0.31	0.88	0.34	0.50
Sedili	1.8	2.8	0.35	0.31	0.56	0.16	0.91
Tioman	2.1	3.5	0.46	0.34	0.60	0.19	1.03
Kuantan	2.0	3.6	0.53	0.36	0.53	0.18	1.26
Cendering	1.5	2.7	0.49	0.31	0.30	0.12	1.90
Geting	0.8	1.4	0.25	0.13	0.17	0.08	1.56

https://doi.org/10.5194/egusphere-2024-294
Preprint. Discussion started: 13 February 2024

References

Antony, C. and Unnikrishnan, A. S.: Observed characteristics of tide-surge interaction along the east coast of India and the head of Bay of Bengal, Estuarine, Coastal and Shelf Science, 131, 6–11, https://doi.org/10.1016/j.ecss.2013.08.004, 2013.

Antony, C., Unnikrishnan, A. S., Krien, Y., Murty, P. L. N., Samiksha, S. V., and Islam, A. K. M. S.: Tide–surge interaction at the head of the Bay of Bengal during Cyclone Aila, Regional Studies in Marine Science, 35, 101 133, https://doi.org/10.1016/j.rsma.2020.101133, 2020.

Arns, A., Wahl, T., Wolff, C., Vafeidis, A. T., Haigh, I. D., Woodworth, P., Niehüser, S., and Jensen, J.: Non-linear interaction modulates global extreme sea levels, coastal flood exposure, and impacts, Nature Communications, 11, 1918, https://doi.org/10.1038/s41467-020-15752-5, 2020.

Buchanan, M. K., Kopp, R. E., Oppenheimer, M., and Tebaldi, C.: Allowances for evolving coastal flood risk under uncertain local sea-level rise, Climatic Change, 137, 347–362, https://doi.org/10.1007/s10584-016-1664-7, 2016.

Calafat, F. M., Wahl, T., Tadesse, M. G., and Sparrow, S. N.: Trends in Europe storm surge extremes match the rate of sea-level rise, Nature, 603, 841–845, https://doi.org/10.1038/s41586-022-04426-5, 2022.

Caldwell, P. C., Merrifield, M. A., and Thompson, P. R.: Sea level measured by tide gauges from global oceans as part of the Joint Archive for Sea Level (JASL) since 1846, https://doi.org/10.7289/V5V40S7W, 2001.

Chen, C., Liu, H., and Beardsley, R.: An Unstructured Grid, Finite-Volume, Three-Dimensional, Primitive Equations Ocean Model: Application to Coastal Ocean and Estuaries, Journal of Atmospheric and Oceanic Technology - J ATMOS OCEAN TECHNOL, 20, 159–186, https://doi.org/10.1175/1520-0426(2003)020<0159:AUGFVT>2.0.CO;2, 2003.

Chen, H., Tkalich, P., Malanotte-Rizzoli, P., and Wei, J.: The forced and free response of the South China Sea to the large-scale monsoon system, Ocean Dynamics, 62, 377–393, https://doi.org/10.1007/s10236-011-0511-7, 2012.

https://doi.org/10.5194/egusphere-2024-294
Preprint. Discussion started: 13 February 2024

Codiga, D.: Unified tidal analysis and prediction using the UTide Matlab functions, Tech. rep., Graduate School of Oceanography, University of Rhode Island, https://doi.org/10.13140/RG.2.1.3761.2008, 2011.

Costa, W., Bryan, K. R., Stephens, S. A., and Coco, G.: A regional analysis of tide-surge interactions during extreme water levels in complex coastal systems of Aotearoa New Zealand, Frontiers in Marine Science, 10, https://www.frontiersin.org/articles/10.3389/fmars.2023. 1170756, 2023.

Diaz, D. B.: Estimating global damages from sea level rise with the Coastal Impact and Adaptation Model (CIAM), Climatic Change, 137, 143–156, https://doi.org/10.1007/s10584-016-1675-4, 2016.

Dixon, M. J. and Tawn, J. A.: Extreme Sea-levels at the UK A-class Sites: Site-by-site Analyses, Proudman Oceanographic Laboratory Internal Document No. 65, https://ntslf.org/sites/ntslf/files/pdf/other_reports/id65.pdf, 1994.

Feng, J., von Storch, H., Jiang, W., and Weisse, R.: Assessing changes in extreme sea levels along the coast of China, Journal of Geophysical Research: Oceans, 120, 8039–8051, https://doi.org/10.1002/2015JC011336, 2015.

Feng, J., Jiang, W., Li, D., Liu, Q., Wang, H., and Liu, K.: Characteristics of tide–surge interaction and its roles in the distribution of surge residuals along the coast of China, Journal of Oceanography, 75, 225–234, https://doi.org/10.1007/s10872-018-0495-8, 2019.

Fernández-Montblanc, T., Vousdoukas, M. I., Ciavola, P., Voukouvalas, E., Mentaschi, L., Breyiannis, G., Feyen, L., and Salamon, P.: Towards robust pan-European storm surge forecasting, Ocean Modelling, 133, 129–144, https://doi.org/10.1016/j.ocemod.2018.12.001, 2019.

GEBCO Compilation Group: The GEBCO_2023 Grid – a continuous terrain model of the global oceans and land, NERC EDS British Oceanographic Data Centre NOC [data set], https://doi.org/10.5285/f98b053b-0cbc-6c23-e053-6c86abc0af7b, 2023.

Haigh, I., Nicholls, R., and Wells, N.: Assessing changes in extreme sea levels: Application to the English Channel, 1900–2006, Continental Shelf Research, 30, 1042–1055, https://doi.org/10.1016/j.csr.2010.02.002, 2010.

Hersbach, H., Bell, B., Berrisford, P., Biavati, G., Horányi, A., Muñoz Sabater, J., Nicolas, J., Peubey, C., Radu, R., Rozum, I., Schepers, D., Simmons, A., Soci, C., Dee, D., and Thépaut, J.-N.: ERA5 hourly data on single levels from 1940 to present, Copernicus Climate Change Service (C3S) Climate Data Store (CDS), https://doi.org/10.24381/cds.adbb2d47, 2018.

Hinkel, J., Lincke, D., Vafeidis, A. T., Perrette, M., Nicholls, R. J., Tol, R. S. J., Marzeion, B., Fettweis, X., Ionescu, C., and Levermann, A.: Coastal flood damage and adaptation costs under 21st century sea-level rise, Proceedings of the National Academy of Sciences, 111, 3292–3297, https://doi.org/10.1073/pnas.1222469111, 2014.

Horsburgh, K. J. and Wilson, C.: Tide-surge interaction and its role in the distribution of surge residuals in the North Sea, Journal of Geophysical Research: Oceans, 112, https://doi.org/10.1029/2006JC004033, 2007.

Hsiang, S., Kopp, R., Jina, A., Rising, J., Delgado, M., Mohan, S., Rasmussen, D. J., Muir-Wood, R., Wilson, P., Oppenheimer, M., Larsen, K., and Houser, T.: Estimating economic damage from climate change in the United States, Science, 356, 1362–1369, https://doi.org/10.1126/science.aal4369, 2017.

Idier, D., Dumas, F., and Muller, H.: Tide-surge interaction in the English Channel, Natural Hazards and Earth System Sciences, 12, 3709–3718, https://doi.org/10.5194/nhess-12-3709-2012, 2012.

Idier, D., Bertin, X., Thompson, P., and Pickering, M. D.: Interactions Between Mean Sea Level, Tide, Surge, Waves and Flooding: Mechanisms and Contributions to Sea Level Variations at the Coast, Surveys in Geophysics, 40, 1603–1630, https://doi.org/10.1007/s10712- 019-09549-5, 2019.

Karri, R. R., Wang, X., and Gerritsen, H.: Ensemble based prediction of water levels and residual currents in Singapore regional waters for operational forecasting, Environmental Modelling Software, 54, 24–38, https://doi.org/10.1016/j.envsoft.2013.12.006, 2014.

Keers, J. F.: An empirical investigation of interaction between storm surge and astronomical tide on the east coast of Great Britain, Deutsche Hydrografische Zeitschrift, 21, 118–125, https://doi.org/10.1007/BF02235726, 1968.

Kurniawan, A., Ooi, S. K., and Babovic, V.: Improved sea level anomaly prediction through combination of data relationship analysis and genetic programming in Singapore Regional Waters, Computers Geosciences, 72, 94–104, https://doi.org/10.1016/j.cageo.2014.07.007, 2014.

https://doi.org/10.5194/egusphere-2024-294
Preprint. Discussion started: 13 February 2024

Kurniawan, A., Tay, S. H. X., Ooi, S. K., Babovic, V., and Gerritsen, H.: Analyzing the physics of non-tidal barotropic sea level anomaly events using multi-scale numerical modelling in Singapore regional waters, Journal of Hydro-environment Research, 9, 404–419, https://doi.org/10.1016/j.jher.2014.10.005, 2015.

Luu, Q.-H., Tkalich, P., Choo, H. K., Wang, J., and Thompson, B.: A storm surge forecasting system for the Singapore Strait, Smart Water, 1, 2, https://doi.org/10.1186/s40713-016-0003-5, 2016.

Marcos, M. and Woodworth, P. L.: Spatiotemporal changes in extreme sea levels along the coasts of the North Atlantic and the Gulf of Mexico, Journal of Geophysical Research: Oceans, 122, 7031–7048, https://doi.org/10.1002/2017JC013065, 2017.

Marzin, C., Rahmat, R., Bernie, D., Bricheno, L., Buonomo, E., Calvert, D., Cannaby, H., Chan, S., Chattopadhyay, M., Cheong, W., et al.: Singapore's second national climate change study–phase 1, chap. 9, E. Met Office, Uk, Centre for Climate Research Singapore, S., National Oceanography Centre, L., UK, Csiro, A. & Newcastle University, N., UK (ed), 2015.

NOAA: Tide and Current Glossary, https://tidesandcurrents.noaa.gov/publications/glossary2.pdf, 2000.

Prandle, D. and Wolf, J.: Surge-Tide Interaction in the Southern North Sea, in: Hydrodynamics of Estuaries and Fjords, edited by Nihoul, J. C., vol. 23 of Elsevier Oceanography Series, pp. 161–185, Elsevier, https://doi.org/10.1016/S0422-9894(08)71277-7, 1978.

Proudman, J.: The propagation of tide and surge in an estuary, Proceedings of the Royal Society of London. Series A. Mathematical and Physical Sciences, 231, 8–24, https://doi.org/10.1098/rspa.1955.0153, 1955.

Proudman, J.: Oscillations of tide and surge in an estuary of finite length, Journal of Fluid Mechanics, 2, 371–382, https://doi.org/10.1017/S002211205700018X, 1957.

Pugh, D. T. and Vassie, J. M.: EXTREME SEA LEVELS FROM TIDE AND SURGE PROBABILITY, Coastal Engineering Proceedings, pp. 52–52, https://doi.org/10.9753/icce.v16.52, 1978.

Pugh, D. T. and Woodworth, P.: Sea-Level Science: Understanding Tides, Surges, Tsunamis and Mean Sea-Level Changes, chap. 4, p. 60–96, Cambridge University Press, https://doi.org/10.1017/CBO9781139235778.007, 2014a.

Pugh, D. T. and Woodworth, P.: Sea-Level Science: Understanding Tides, Surges, Tsunamis and Mean Sea-Level Changes, chap. 7, p. 155–188, Cambridge University Press, https://doi.org/10.1017/CBO9781139235778.010, 2014b.

Rasmussen, D. J., Bittermann, K., Buchanan, M. K., Kulp, S., Strauss, B. H., Kopp, R. E., and Oppenheimer, M.: Extreme sea level implications of 1.5 °C, 2.0 °C, and 2.5 °C temperature stabilization targets in the 21st and 22nd centuries, Environmental Research Letters, 13, 034 040, https://doi.org/10.1088/1748-9326/aaac87, 2018.

Rossiter, J. R.: Interaction Between Tide and Surge in the Thames, Geophysical Journal International, 6, 29–53, https://doi.org/10.1111/j.1-246X.1961.tb02960.x, 1961. 1

Searson, D. P., Leahy, D., and Willis, M.: GPTIPS:An Open Source Genetic Programming Toolbox For Multigene Symbolic Regression, Lecture Notes in Engineering and Computer Science, 2180, 2010.

Sreeraj, P., Swapna, P., Krishnan, R., Nidheesh, A. G., and Sandeep, N.: Extreme sea level rise along the Indian Ocean coastline: observations and 21st century projections, Environmental Research Letters, 17, 114 016, https://doi.org/10.1088/1748-9326/ac97f5, 2022.

Tay, S. H. X., Kurniawan, A., Ooi, S. K., and Babovic, V.: Sea level anomalies in straits of Malacca and Singapore, Applied Ocean Research, 58, 104–117, https://doi.org/10.1016/j.apor.2016.04.003, 2016.

Tkalich, P., Vethamony, P., Babu, M. T., and Malanotte-Rizzoli, P.: Storm surges in the Singapore Strait due to winds in the South China Sea, Natural Hazards, 66, 1345–1362, https://doi.org/10.1007/s11069-012-0211-8, 2013a.

Tkalich, P., Vethamony, P., Luu, Q.-H., and Babu, M. T.: Sea level trend and variability in the Singapore Strait, Ocean Science, 9, 293–300, https://doi.org/10.5194/os-9-293-2013, 2013b.

van Maren, D. S. and Gerritsen, H.: Residual flow and tidal asymmetry in the Singapore Strait, with implications for resuspension and residual transport of sediment, Journal of Geophysical Research: Oceans, 117, https://doi.org/10.1029/2011JC007615, 2012.

von Storch, H., Jiang, W., and Furmanczyk, K. K.: Chapter 7 - Storm Surge Case Studies, in: Coastal and Marine Hazards, Risks, and Disasters, edited by Shroder, J. F., Ellis, J. T., and Sherman, D. J.,

https://doi.org/10.5194/egusphere-2024-294
Preprint. Discussion started: 13 February 2024

Hazards and Disasters Series, pp. 181–196, Elsevier, Boston, https://doi.org/10.1016/B978-0-12-396483-0.00007-8, 2015.

Wolf, J.: Interaction of tide and surge in a semi-infinite uniform channel, with application to surge propagation down the east coast of Britain, Applied Mathematical Modelling, 2, 245–253, https://doi.org/10.1016/0307-904X(78)90017-3, 1978.

Wolf, J.: Surge-tide interaction in the North Sea and River Thames, Floods Due to High Winds and Tides, pp. 75–94, 1981.

Woodworth, P. L. and Blackman, D. L.: Evidence for Systematic Changes in Extreme High Waters since the Mid-1970s, Journal of Climate, 17, 1190–1197, https://doi.org/10.1175/1520-0442(2004)0172.0.CO;2, 2004.

Wróbel-Nied´zwiecka, I., Drozdowska, V., and Piskozub, J.: Effect of drag coefficient formula choice on wind stress climatology in the North Atlantic and the European Arctic, Oceanologia, 61, 291–299, https://doi.org/10.1016/j.oceano.2019.02.002, 2019.

Yaakob, O., Hashim, F. E., Mohd Omar, K., Md Din, A. H., and Koh, K. K.: Satellite-based wave data and wave energy resource assessment for South China Sea, Renewable Energy, 88, 359–371, https://doi.org/10.1016/j.renene.2015.11.039, 2016.

Yang, S., Sheng, J., Ohashi, K., Yang, B., Chen, S., and Xing, J.: Non-linear interactions between tides and storm surges during extreme weather events over the eastern Canadian shelf, Ocean Dynamics, 73, 279–301, https://doi.org/10.1007/s10236-023-01556-w, 2023.

Zhang, X., Chu, D., and Zhang, J.: Effects of nonlinear terms and topography in a storm surge model along the southeastern coast of China: a case study of Typhoon Chan-hom, Natural Hazards, 107, 551–574, https://doi.org/10.1007/s11069-021-04595-y, 2021.